CCS Chemistry

RESEARCH ARTICLE

Received: Jan. 25, 2021 | Accepted: Apr. 6, 2021

Fine-Tuning Contact via Complexation for High-Performance Organic Solar Cells

Yawen Li[1†], Zhenzhen Zhang[1,2†], Xiaona Han[1†], Tao Li[3*] & Yuze Lin[1,2*]

[1]*Beijing National Laboratory for Molecular Sciences, CAS Key Laboratory of Organic Solids, Institute of Chemistry, Chinese Academy of Sciences, Beijing 100190,* [2]*University of Chinese Academy of Sciences, Beijing 100049,* [3]*Center for Spintronics and Quantum Systems, State Key Laboratory for Mechanical Behavior of Materials, Department of Materials Science and Engineering, Xi'an Jiaotong University, Xi'an, Shaanxi 710049*

[*]*Corresponding authors: linyz@iccas.ac.cn; taoli66@xjtu.edu.cn;* [†]Y. Li, Z. Zhang, and X. Han contributed equally to this work.

Cite this: *CCS Chem.* **2021**, *3*, 1206–1216

For organic optoelectronic devices, precise tuning of the electrical property of both active layers and interfaces is crucial to achieve enhanced device performance. Herein, we developed a facile method using complexation to modify the work function and energy levels of cathode contact layers in organic solar cells (OSCs) to achieve suitable work function and energy levels while retaining relatively good conductivity. Compared with the control devices with neat (*N,N*-dimethyl-ammonium *N*-oxide)propyl perylene diimide (PDINO) contacts, the tris(pentafluorophenyl)borane (BCF)-complexed PDINO cathode contacts showed enhanced power conversion efficiencies (PCEs), which is independent of the composition of the active layer. More specifically, single-junction OSCs employing PDINO cathode contact with 2 wt % BCF-additive achieved an average PCE of 17.7%. Based on experimental data and theoretical modeling, we found that the boron cores of BCF coordinate with the amino *N*-oxide terminal substituent of PDINO after generating BCF–H_2O/methanol complexes. BCF segments with a strong electron-withdrawing property can effectively reduce the energy levels of the PDINO–BCF complex, and thus enhance device PCE when it is used as a cathode contact in OSCs. This strategy can be extended to other types of photovoltaic devices, photodetectors, and light-emitting diodes.

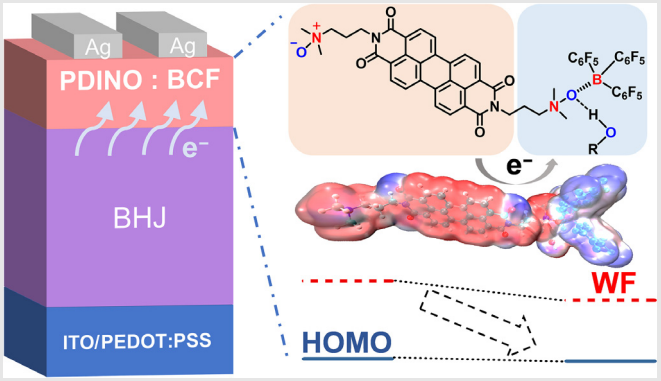

Keywords: **organic solar cells, interface, cathode contact, complexation, work function**

Introduction

Precisely manipulating the electrical properties, such as charge carrier density, conductivity, energy level, and work function, of semiconductors is one of the underpinnings of inorganic and organic electronics, such as solar cells, field-effect transistors, light-emitting diodes, and others.[1-5] Organic solar cells (OSCs) are promising cost-effective, light-weight alternatives to silicon-based solar cells for certain applications.[5-16] Plentiful active layer materials, such as PM6,[17] PM7,[18] PM6-Tz20,[19] PTQ10,[20] D18,[21] M34,[22] Y6,[23] BTP-4Cl,[24] and their analogues, have been explored to

DOI: 10.31635/ccschem.021.202100832
CCS Chem. **2021**, *3*, 1206–1216

boost the efficiency of OSCs to over 16%.[25] In contrast, it is more challenging to develop efficient contact materials (interface materials) with all requirements of high conductivity, proper work function and energy levels, orthogonal solubility, and so forth. Very few types of efficient organic semiconducting contacts have been employed for high-performance OSCs.[26–28] In addition to the design and synthesis of new efficient contact materials, it is necessary to develop facile strategies to modify currently available materials for optimized energy level alignment, reduced series resistance, and finally improved device performance in OSCs and other optoelectronic applications.[29,30]

Herein, we developed a convenient method of introducing tris(pentafluorophenyl)borane (BCF) into the cathode layer to tune energy level alignment within devices. OSCs employing (*N*,*N*-dimethyl-ammonium

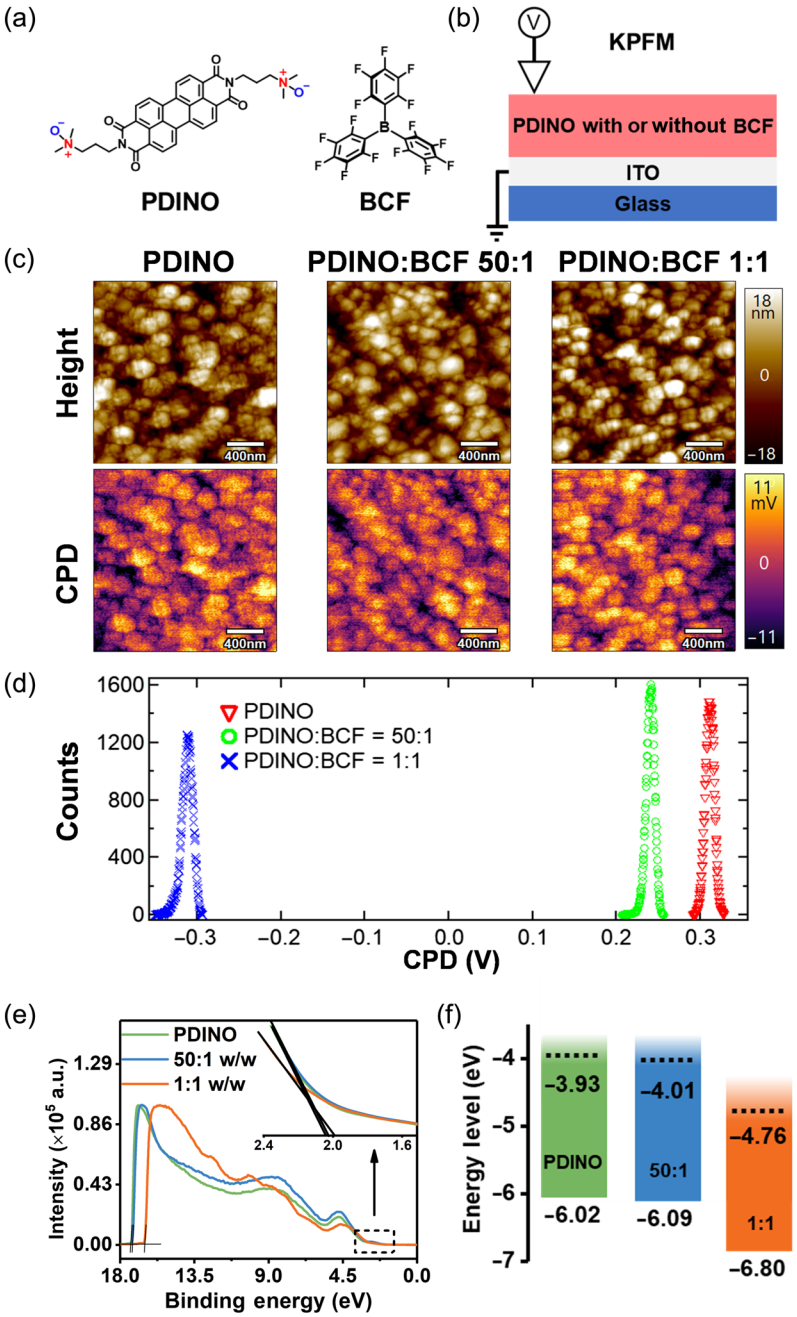

Figure 1 | *Work function and energy level characterizations. (a) Chemical structures of PDINO and BCF. (b) Setup scheme of KPFM measurement. (c) Morphology and CPD distribution images of the PDINO, PDINO:BCF (50:1, w/w), and PDINO:BCF (1:1, w/w) films. (d) Histograms of CPD images. (e) UPS spectra of the PDINO, PDINO:BCF (50:1, w/w), and PDINO:BCF (1:1, w/w) films. (f) Energy diagram of the PDINO, PDINO:BCF (50:1, w/w), and PDINO:BCF (1:1, w/w) films. Dash lines indicate work function.*

DOI: 10.31635/ccschem.021.202100832
CCS Chem. **2021**, *3*, 1206–1216

N-oxide)propyl perylene diimide (PDINO) with BCF additive (Figure 1a) as cathode contacts show enhanced device power conversion efficiencies (PCEs) relative to the control devices with neat PDINO contacts, independent of the composition of the active layer. Among them, D18:Y6-based OSCs with the PDINO–BCF contact show average PCE of 17.7%, which is one of the highest values reported for single-junction OSCs to date.[21] The complex of PDINO–BCF–H_2O/methanol is formed in the PDINO–BCF blend layers, in which the BCF segment with a strong electron-withdrawing property reduces the electron density of the π-system of the PDINO segment, resulting in the lowering of cathode layer energy levels and thus enhancing device efficiency of OSCs.

Experimental Methods

Fabrication of solar cell devices

OSCs were fabricated with the structure of indium tin oxide (ITO)/poly(3,4-ethylenedioxythiophene) (PEDOT):poly(styrenesulphonate) (PSS)/active layer/PDINO with and without BCF/Al or Ag. The patterned ITO glass was cleaned by sonication for 30 min independently in deionized water, acetone, and isopropanol. After patterned ITO glass was treated in an UV-ozone chamber (SunMonde Company, Shanghai, China) for 5 min, a hole-transporting layer of PEDOT:PSS (Clevios VP AI 4083, Heraeus, Leverkusen, Germany) was deposited by the spin-coating solution at 4000 rpm for 30 s, followed by thermal annealing at 150 °C for 20 min. A solution of donor:acceptor blend was subsequently spin-coated on the PEDOT:PSS layer to form a photosensitive layer. Then PDINO with and without BCF additive in methanol solution (1 mg mL^{-1}) was coated on the top of the active layer by spin coating at 3000 rpm for 30 s. The BCF first was dissolved in methanol, and then added to the PDINO methanol solution using micropipette. The solution was mixed for at least 30 min and then used. Finally, Al or Ag was evaporated onto the surface under vacuum (ca. 10^{-5} Pa). The active area of the device was 4 mm^2. The current density–voltage (*J*–*V*) curves were measured under AM 1.5G light at 100 mW cm^{-2}.

The details of characterization are presented in the Supporting Information.

Results and Discussion

PDINO has been one of the most widely used solution-processed cathode contacts for high-performance OSCs.[20,31–35] However, the lowest unoccupied molecular orbital (LUMO) energy level of PDINO of approximately –3.7 eV[26] is higher than those (–3.85 to –4.0 eV) of the popular electron acceptors like $PC_{71}BM$, (3,9-bis(2-methylene-(3-(1,1-dicyanomethylene)-indanone))-5,5,11,11-tetrakis(4-hexylphenyl)-dithieno[2,3-d:2′,3′-d′]-s-indaceno[1,2-b:5,6-b′]dithiophene) (ITIC), and Y6.[13,23,36] These mismatched energy levels between PDINO and the widely used electron acceptors indicate that the device performance of OSCs based on PDINO cathode contacts could be further enhanced by eliminating the LUMO energy barrier between PDINO and the active layer. BCF, as a typical and widely used p-type dopant, is able to move down the energy levels and work function of many organic molecules and polymer semiconductors for organic electronics,[37–44] which drives us to investigate how BCF additive affects the electronic property of contact layers, like PDINO. To investigate the effect of BCF additive on the electronic property of the PDINO thin film, the work function and energy levels of PDINO thin film with and without BCF additive were acquired by using Kelvin probe force microscopy (KPFM), and UV photoelectron spectroscopy (UPS).

KPFM is a surface potential microscopy that is a non-contact variant of atomic force microscopy (AFM). By KPFM, the surface potential and effective work function of metal or semiconductor surfaces can be observed at atomic or molecular scales.[45] The measured effective work function relates to many surface phenomena, including doping and band bending of semiconductors.[46] KPFM can reflect information about the composition and electronic state of the local structures on the surface of a solid by mapping the effective work function of the detected surface.[47] Here, the setup scheme of KPFM measurement is shown in Figure 1b. In Figure 1c, the PDINO films with and without BCF additive are composed of nanograins as determined by KPFM. The root-mean-square roughness values of PDINO neat films, PDINO:BCF (50:1, w/w) blend film, and PDINO:BCF (1:1, w/w) blend film are 7.5, 7.8, and 8.6 nm, respectively. The spatial distributions of contact potential difference (CPD) of the three samples are rather uniform, but the absolute average CPD values differ dramatically among them. The CPD reflects the relative work function with respect to that of the tip (Pt/Ir-coated conductive silicon probe), which is defined as $(\Phi_{tip} - \Phi_{sample})/e$ (Φ_{tip} and Φ_{sample} are the tip and sample work functions, respectively, and e is the elementary charge).[48] Taking the work function of the tip as a reference, the work function increases with the content of BCF. The work function of PDINO:BCF blended film with a weight ratio of 50:1 and 1:1 is approximately 0.1 and 0.6 V, respectively, higher than that of the pure PDINO thin film (Figure 1d).

UPS measurement shows that BCF additive increases the work function and moves down the highest occupied molecular orbital (HOMO) energy level of PDINO. The neat PDINO thin film shows a work function of 3.93 eV and HOMO level of –6.02 eV (Figures 1e and 1f). PDINO:BCF blend film with 2 wt % BCF additive shows a higher work function of 4.01 eV with a lower HOMO level of –6.09 eV. As the BCF content in PDINO increases to 1:1, the work function of the PDINO:BCF blend film further

DOI: 10.31635/ccschem.021.202100832
CCS Chem. **2021**, *3*, 1206–1216

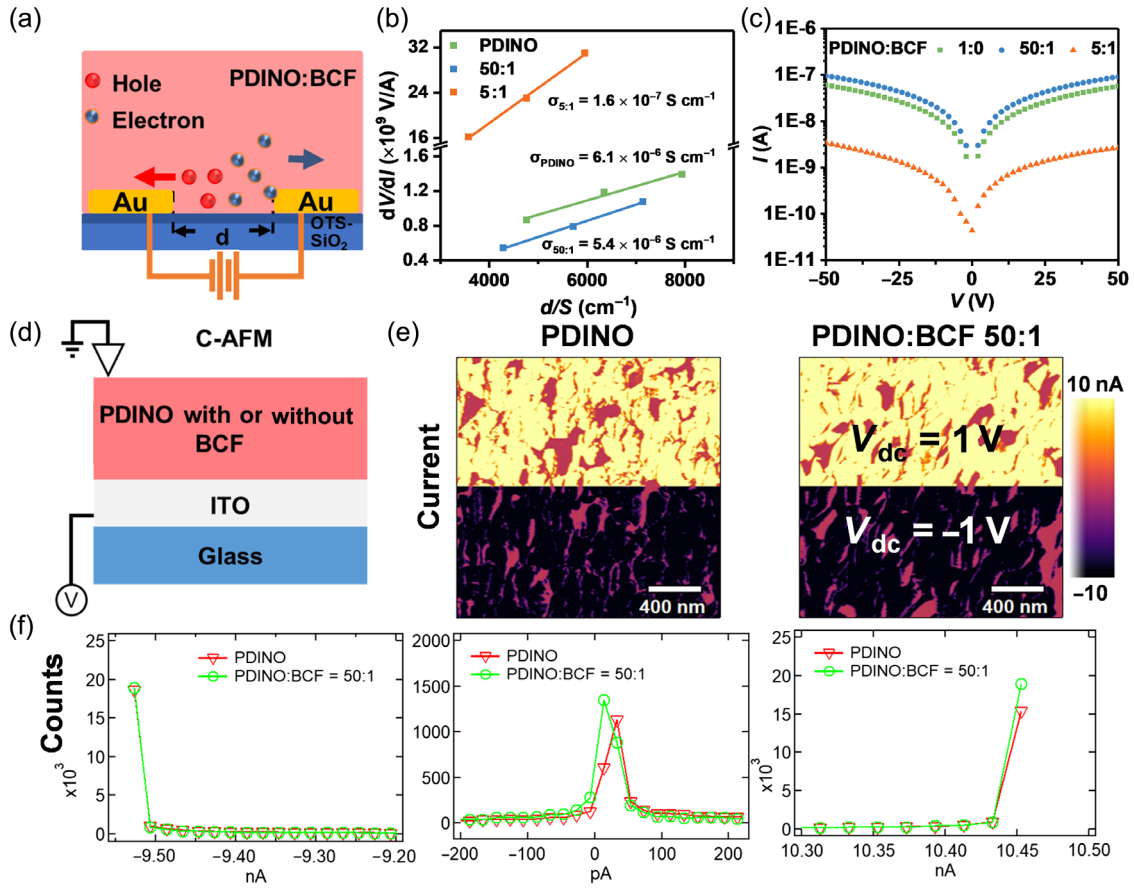

Figure 2 | *Charge-transporting property of PDINO with and without BCF. (a) Scheme of the device setup for conductivity measurement. (b) dV/dI vs d/S plots and calculated conductivity of PDINO and PDINO:BCF blend films (50:1, 5:1 w/w). (c) I–V characteristics of PDINO and PDINO:BCF blend films (50:1, 5:1 w/w) with channel widths of 30 μm. (d) Setup scheme of C-AFM measurement. (e) Vertical dark-current images of C-AFM. (f) Dark current extracted from C-AFM images.*

increases to 4.76 eV with a much lower HOMO level of –6.80 eV. This result from UPS observation is consistent with the KPFM results. These results indicate that BCF can efficiently move down the work function and HOMO energy levels of the PDINO film. Then the LUMO energy of the PDINO film should also be lower as an accompanying effect of the moving down HOMO because of the relatively fixed optical bandgap of PDINO (Supporting Information Figure S1).

After we demonstrated that BCF moves down both work function and energy levels of PDINO film, the conductivity of PDINO film with and without BCF additive was investigated by two probe measurements on lateral devices, in which the varied channel lengths were used to exclude the effect of contact resistances, respectively. The lateral device structure is illustrated in Figure 2a and consisted of two gold electrodes deposited on insulated SiO_2 substrates covered by PDINO and PDINO:BCF blend film. The length of electrodes was 1400 μm, and varied channel widths of 30, 40, and 50 μm were used. In Figure 2b, the calculated conductivity of neat PDINO film is 6.1×10^{-6} S cm^{-1}; the PDINO:BCF blend film (50:1, w/w) showed similar conductivity of 5.4×10^{-6} S cm^{-1}; and the PDINO:BCF blend film (5:1, w/w) showed over one order lower conductivity of 1.6×10^{-7} S cm^{-1}. Although 2 wt % BCF additive decreases conductivity, the dark current of lateral devices based on PDINO:BCF (50:1, w/w) blend film is higher than the device based on neat PDINO film (Figure 2c). This phenomenon can be explained by reduced contact resistance between the PDINO:BCF film and metal electrodes, due to their better energy alignment. The electron mobility within blend films was calculated from the space-charge-limited current (SCLC) method employing an electron-only device structure of ITO/ZnO/PDINO or PDINO:BCF blend film/Al. The neat PDINO thin film exhibits electron mobility of 1.7×10^{-5} cm^2 V^{-1} s^{-1}, and the PDINO:BCF blend film with a weight ratio of 50:1 shows increased electron mobility of 3.4×10^{-5} cm^2 V^{-1} s^{-1} (Supporting Information Figure S2). Here, the increased charge-carrier mobility of PDINO induced by 2% BCF additive is consistent with what is observed in literature.[37,43]

DOI: 10.31635/ccschem.021.202100832
CCS Chem. **2021**, *3*, 1206–1216

We also used conductive AFM (C-AFM) to investigate the vertical conductivity of PDINO film with and without BCF additive. The C-AFM can simultaneously measure the surface topography of the sample and the electric current flow across the sample thickness.[49] The C-AFM of PDINO film with and without 2 wt % BCF was measured by contact mode (Figure 2d), in which the ITO is the bottom electrode and the platinum-coated tip works as the top electrode. In Figure 2e, both the films show high dark currents except for a few grain boundaries. Figure 2f reveals that PDINO film with 2 wt % BCF exhibits a slightly higher dark current than that of the neat PDINO thin film at the same bias of ±1 V. This result indicates that the small quantity of BCF additive did not obviously change the conductivity of PDINO film on a vertical direction to the substrate but did tune the work function and energy level of PDINO causing a lower contact resistance within devices.

Since PDINO with optimized BCF amounts shows optimized energy level and work function while maintaining good conductivity, one of its promising applications is the use in high-performance solar cells as a cathode contact layer to modify the contact between active layer and electrodes. To demonstrate its potential, we fabricated OSCs with a device structure of ITO/PEDOT:PSS/organic bulk heterojunction (BHJ) photoactive layer/PDINO with and without BCF/metal cathode (Al or Ag) (Figure 3a). First, we selected the typical polymer donor PTB7-Th and fullerene acceptor $PC_{71}BM$ as the BHJ layer (Supporting Information Figure S3). The corresponding photovoltaic data, as well as device efficiencies of the OSC devices with optimized PTB7-Th:$PC_{71}BM$ blends using PDINO with varied amounts of BCF additive as cathode contacts under the illumination of AM 1.5G, 100 mW cm^{-2}, are listed in Supporting Information Table S1 (Supporting Information Figure S4). The devices with neat PDINO as the cathode interfacial materials deliver a PCE of 5.9% with an open-circuit voltage (V_{oc}) of 0.800 V, short-circuit current density (J_{sc}) of 13.6 mA cm^{-2}, and fill factor (FF) of 53.5%. The PDINO with an addition of 2 wt % BCF displays an increased PCE of 6.7% (V_{oc} = 0.809 V, J_{sc} = 14.2 mA cm^{-2}, FF = 58.2%). We found that the J_{sc} increases from 13.6 to 14.2 mA cm^{-2} and FF increases from 53.5% to 58.2%, which can be attributed to the better electron extraction of cathode electrodes. To test the universality of the PDINO with BCF cathode contact for OSCs fabricated with other active layers, devices were fabricated with high-performance

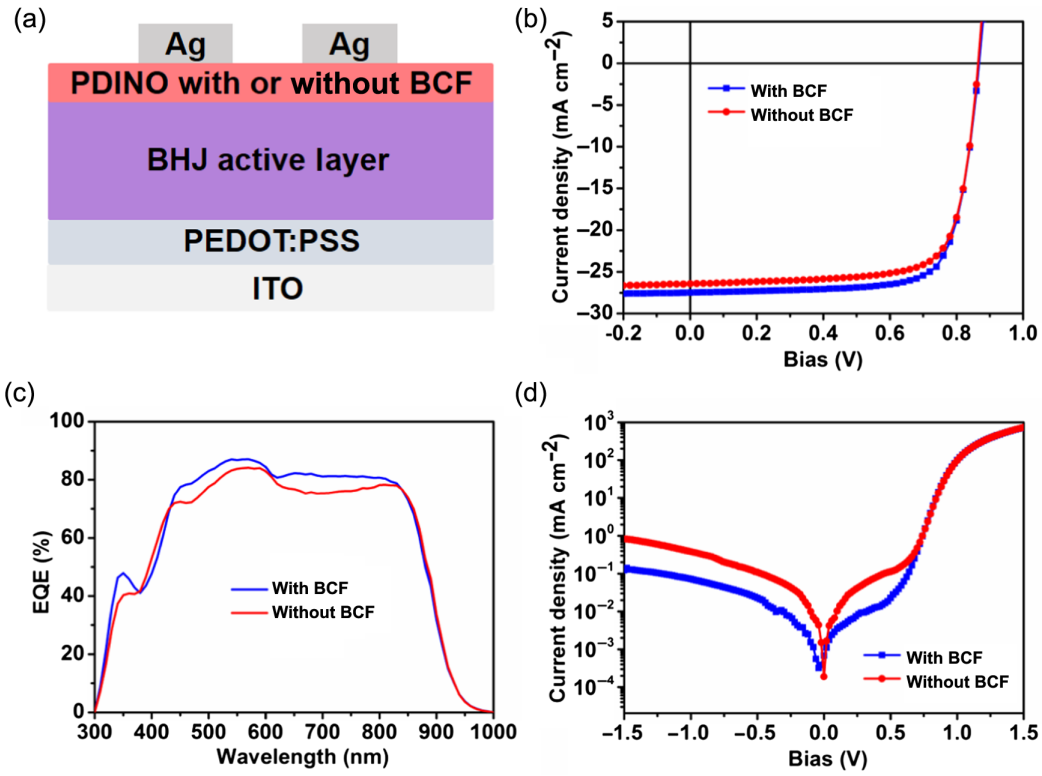

Figure 3 | *Photovoltaic performance of the OSCs employing PDINO with and without BCF. (a) Device structure of the OSCs. (b) J–V curves of the best OSCs based on D18:Y6 blend using PDINO film with and without 2 wt % BCF as cathode contact layer under the illumination of AM 1.5G, 100 mW cm^{-2}. (c) EQE spectra of the best OSCs based on D18:Y6 blend using PDINO film with and without 2 wt % BCF as a cathode contact layer. (d) Dark currents of the best OSCs based on D18:Y6 blend using PDINO film with and without 2 wt % BCF as a cathode contact layer.*

DOI: 10.31635/ccschem.021.202100832
CCS Chem. **2021**, *3*, 1206–1216

nonfullerene BHJ absorbers consisting of PM6:Y6:IDIC[50] as the ternary component and D18:Y6 as binary component (Supporting Information Figure S3). Like PTB7-Th:$PC_{71}BM$-based OSCs, the PDINO:BCF cathode contact improves the efficiencies of PM6:Y6:IDIC and D18:Y6-based devices. Relative to the control device with neat PDINO contact, 2 wt % BCF increases the PCE from 15.4% to 15.8% in PM6:Y6:IDIC-based OSCs (Supporting Information Figure S4 and Table S1). D18:Y6-based binary OSCs with 2 wt % BCF added PDINO contact shows an average PCE of 17.7% for eight devices, with the best value of 18.1% (Figure 3b), a V_{oc} of 0.865 V, J_{sc} of 27.5 mA cm^{-2}, and FF of 75.9%. In contrast, the control device based on D18:Y6 active layer with neat PDINO contact shows a relatively low PCE of 17.1% (with an average value of 16.9%). The PCEs achieved in our devices with the PDINO:BCF contact are among the best values reported for single-junction OSCs to date.[21,24,51–54] It should be noted that the BCF additive in PDINO film may slightly affect the morphology and electronic property on the surface layer of the BHJ active layer[55,56] because of likely direct contact between the active layer and proximate BCF. Figure 3c shows that the external quantum efficiency (EQE) spectrum of the devices based on D18:Y6 active layer and PDINO contact with 2 wt % BCF additive is higher than that of the control devices without BCF additive. The photocurrent density calculated from EQE was <5% mismatch from those of the *J*–*V* measurement, which is among the reasonable mismatched values reported for high-performance OSCs.[57,58] Figure 3d shows D18:Y6-based OSCs employed with PDINO layer with 2 wt % BCF yield lower dark current density relative to the control devices based on neat PDINO cathode contact. These results are consistent with PDINO with 2 wt % BCF additive being a better cathode contact than the neat PDINO layer. We also measured the shelf-, thermal-, and photostability of devices with PDINO or PDINO:BCF (50:1, w/w) contact and found that BCF did not obviously affect device stabilities (Supporting Information Figure S5).

The next question to be addressed is how the BCF interacts with PDINO to tune the electronic property of the PDINO and finally improves the device performance when acting as cathode contacts. Very recently, a comprehensive mechanism of BCF p-doping thiophene-related polymer and organic semiconductors has been well demonstrated where p-type doping occurred between polymers and BCF–H_2O complex. The BCF–H_2O complex as a Brønsted acid protonates the polymer backbone followed by electron transfers from a neutral chain segment to a positively charged, protonated one, forming a Lewis acid-base adduct.[37] This protonic acid doping by BCF–H_2O complex generally occurs in organic and polymeric semiconductors in the presence of a thiophene-related moiety, which usually behaves as a p-type and Lewis basic property. However, it is still unknown how the BCF interacts with other types of organic semiconductors that do not consist of any thiophene-related moiety, including the PDINO we used here.

To reveal the mechanism of interaction between PDINO and BCF, the electrospray ionization mass spectrometry (ESI-MS), ^{19}F nuclear magnetic resonance (^{19}F-NMR), UV–vis absorption spectroscopy, Fourier transform infrared (FTIR) spectroscopy, and X-ray photoelectron spectroscopy (XPS) measurements were conducted to analyze the PDINO–BCF mixture.

ESI-MS is a MS technique that produces ions using an electrospray in which a high voltage is applied to transform a liquid to an aerosol. This soft ionization technique overcomes the propensity of molecules to fragment when ionized, thus it is especially useful in producing ions from macromolecules and coordination compounds. ESI-MS of BCF from methanol solution showed a very weak molecule weight peak of BCF molecule, which indicates most BCF molecules reacted or strongly interacted with others in solution. Instead, we attribute two *m*/*z* values with a single negative charge (M^-) at 529 and 543 (Figure 4a) to a BCF–H_2O complex and BCF–methanol complex, respectively. This result indicates BCF can form a complex with methanol, along with an unavoidable trace of moisture or water in air or solvent. Then the ^{19}F NMR spectra of BCF in methanol–D4 solution show two independent groups of peaks (Figure 4b), which are consistent with that of the BCF–methanol complex and BCF–H_2O complex formed. Then ESI-MS from PDINO:BCF mixed methanol solution shows *m*/*z* of 593 (M^{2+}), 1123 (M^+), and 1137(M^+), which are assigned to PDINO dimer, PDINO–BCF–H_2O complex, and PDINO–BCF–methanol complex, respectively. These results indicate that PDINO easily forms complexes with BCF–H_2O/methanol complex, and the interaction between PDINO and BCF–H_2O/methanol is relatively strong so that they generate air-stable ions detectable by MS detectors. ^{19}F NMR spectra of BCF in PDINO:BCF mixed methanol–D4 solution show new sets of F atoms, and each set includes three chemical shifts of F at the ortho-, meta-, para-sites on the benzene rings. B and F sites on the BCF are possible sites to interact with PDINO. If the F atom coordinated with PDINO, it is highly possible the molecular symmetry of BCF is lost, leading to an additional chemical shift of F atom. Thus, the new set of three chemical shifts of F atoms in PDINO:BCF mixture denotes B atoms, not F atoms, is the more likely site of the BCF interacting with PDINO.

Then we used UV–vis absorption and FTIR spectroscopy to investigate which sites of PDINO interact with the boron cores of BCF. According to previous studies,[38,40] in a mixture of BCF and thiophene-related polymers, the addition of BCF resulted in a clear decrease in the optical bandgap of those polymers and induced new absorption at long wavelength caused by polaron.[37,41] The UV–vis

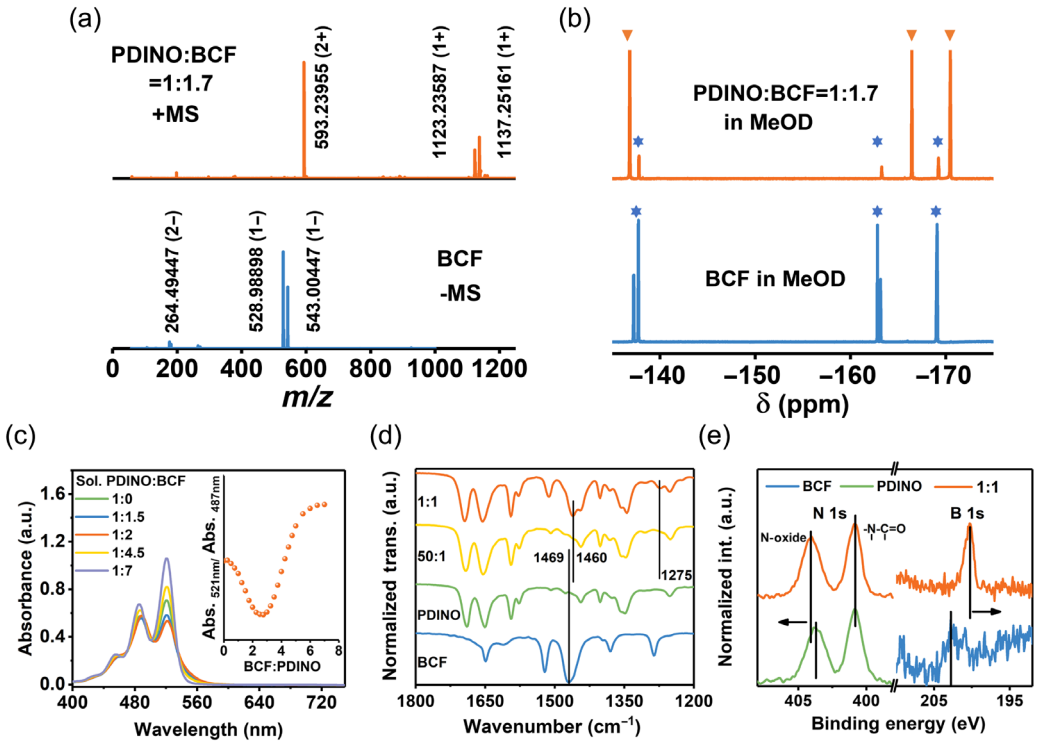

Figure 4 | *Characterization of the interaction between PDINO and BCF. (a) ESI-MS of BCF and PDINO:BCF mixture (1:1.7, w/w). (b) [19]F NMR of BCF and PDINO:BCF mixture (1:1.7, w/w). (c) UV–vis absorption spectroscopy of PDINO:BCF mixture (w/w) in methanol. Insert describes the relative intensity variation of 521 vs 487 nm from PDINO:BCF from 1:0 to 1:7 (w/w). (d) FTIR spectroscopy of BCF and PDINO:BCF mixture (w/w). (e) XPS of BCF and PDINO:BCF mixture (1:1, w/w).*

absorption spectra of PDINO in methanol solution with and without a varied amount of BCF additive were measured. In Figure 4c, PDINO methanol solutions show three typical absorption peaks which are dominated by characteristic π–π* transitions. Compared with thiophene-related polymers, BCF does not obviously narrow the optical bandgap nor change the peak shape of PDINO in solution. However, the PDINO solution with BCF addition shows an obvious change in peak intensity. Relative to the neat PDINO methanol solution, upon increasing the BCF amount in PDINO, the 521 nm absorption peak first decreases and then increases as the weight ratio of PDINO to BCF nears 1:2.5. These changes in absorption shape and intensity of PDINO indicate the existence of the interaction between PDINO and BCF might affect the self-aggregation of PDINO in solution.[59] Then both the simple perylene and perylene diimide (PDI-C11) with alkyl side chains (Supporting Information Figure S6) were induced as reference molecules to investigate UV–vis absorption before and after adding BCF. Compared with the PDINO solution, BCF additive has a negligible effect on the absorption peak shape and intensity of perylene or PDI-C11 in chloroform solution, which indicates there is no detectable interaction between Lewis acid BCF and perylene/PDI-C11, even though the PDI-C11 provides four Lewis base carbonyl (C=O) groups. We further added BCF methanol solution, in which a Brønsted acid complex with BCF forms, into perylene/PDI-C11 chloroform solution, which still could not induce any detectable absorption change. By comparing the chemical structures of perylene, PDI-C11, and PDINO, ammonium *N*-oxide end groups of PDINO are the potential sites to interact with BCF or BCF–H_2O/methanol complex.

From the FTIR analysis in Figure 4d, we found a new peak at the wavenumber of 1275 cm^{-1} in PDINO:BCF mixture with a weight ratio of 1:1, which is attributed to B–O–N stretching vibrations according to the literature.[60] The FTIR results further confirm the PDINO:BCF complex formation and support the ammonium *N*-oxide end groups of PDINO and B atom of BCF are the sites interacting with each other, which are consistent with the results of UV–vis absorption and the NMR of PDINO:BCF mixture. Meanwhile, the peak value of B–C of BCF stretching vibration shifts from 1469 cm^{-1} of BCF to 1460 cm^{-1} of PDINO:BCF blend, and this shift supports the effect of electron donating from PDINO to the B atom of BCF.[61] The XPS results provide evidences to further support this electron transfer effect from PDINO to BCF. In Figure 4e, PDINO:BCF (1:1, w/w) blend shows decreased binding energy of B 1s relative to that of the neat BCF film (202.8–200.3 eV), along with

DOI: 10.31635/ccschem.021.202100832
CCS Chem. **2021**, *3*, 1206–1216

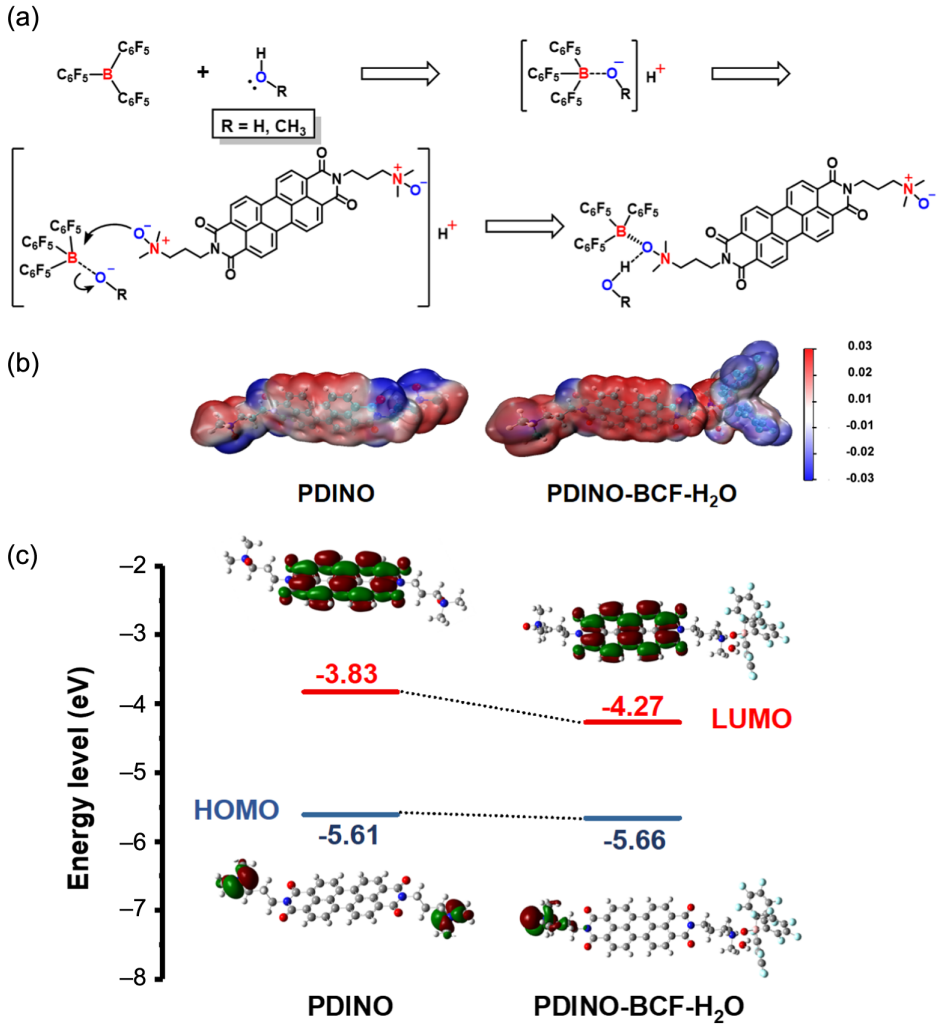

Figure 5 | *Interaction mechanism between PDINO and BCF, and density functional theory (DFT) analysis. (a) Schematic of the interaction between PDINO and BCF. (b) Molecular electrostatic potentials (MEPs) on the 0.001 au electron density isosurface of isolated PDINO and PDINO-BCF-H_2O complex by DFT calculation at the B3LYP/6-31G+(d,p) level. (c) Frontier orbitals energy level of PDINO and PDINO–BCF–H_2O complex by DFT calculation at the B3LYP/6-31G+(d,p) level.*

increased N 1s binding energy of the *N*-oxide terminal relative to that of neat PDINO film (403.7–404.1 eV).[35] Meanwhile, the binding energy attributed to the N 1s of the imide remained constant (400.8 eV) after adding BCF to PDINO film. These results further confirm that the *N*-oxide terminals on PDINO are the sites interacting with BCF. Electron transfer from PDINO to BCF through the complexation is expected to contribute to the lower energy levels and work function of PDINO film by BCF.

Finally, we propose the working principle of BCF tuned electronic property of PDINO. As shown in Figure 5a, the BCF initially complexes with water and methanol to form the Brønsted acid and then coordinates with ammonium *N*-oxide of PDINO. PDINO donates electrons to BCF through the B–O–N bond within the PDINO–BCF complex. The density functional theory (DFT) approach was applied to calculate the electron-density distribution, LUMO, and HOMO levels of PDINO and PDINO–BCF–H_2O complex. Relative to that of neat PDINO, the PDINO segment in the PDINO–BCF–H_2O complex shows lower electron density, which is attributed to the strong electron-withdrawing property of the BCF segment (Figure 5b). As a result, the calculated LUMO and HOMO of PDINO–BCF–H_2O complex are –4.27 and –5.66 eV separately, which are lower than that of PDINO (–3.83 eV for LUMO and –5.61 eV for HOMO) (Figure 5c). The decrease of frontier molecular orbitals of PDINO–BCF complex is consistent with what we observed in our experimental measurements and further proves our acting principle of BCF interacting with PDINO to decrease its energy levels.

DOI: 10.31635/ccschem.021.202100832
CCS Chem. **2021**, *3*, 1206–1216

Conclusion

We tuned the work function and energy levels of cathode contact material through a convenient complexation to optimize energy alignment, and thus boosted the device efficiency of OSCs. Relative to the neat PDINO film, the PDINO modified by 2 wt % BCF exhibited lower energy levels while maintaining relatively good conductivity. When PDINO:BCF blend was used as a cathode contact in OSCs, device PCEs were improved compared with devices with neat PDINO contact, independent of the photoactive layer of OSCs. Then, through experimental and theoretical analysis, we proposed the mechanism of BCF interacting with PDINO through complex formation. The electron transfers from PDINO to BCF through the B–O–N bond formed in PDINO–BCF–H_2O/methanol complexes. Our work suggests the more facile and economical strategy of tuning the existing contact layers via complexation, relative to developing new contact materials, can be very promising to improve device performance of OSCs, and we predict this strategy can be extended to other types of solar cell devices like perovskite solar cells as well as other types of optoelectronics.

Supporting Information

Supporting Information is available and includes experimental procedures and details, Figures S1–S6, and Table S1.

Conflict of Interest

There is no conflict of interest to report.

Funding Information

The authors thank the National Key R&D Program of China (no. 2018YFB0407601), the National Natural Science Foundation of China (no. 51802250), the Key R&D Program of Shanxi (no. 2019TSLGY08), and Chinese Academy of Sciences.

References

1. Tang, C. G.; Ang, M. C.; Choo, K. K.; Keerthi, V.; Tan, J. K.; Syafiqah, M. N.; Kugler, T.; Burroughes, J. H.; Png, R. Q.; Chua, L. L.; Ho, P. K. Doped Polymer Semiconductors with Ultrahigh and Ultralow Work Functions for Ohmic Contacts. *Nature* **2016**, *539*, 536–540.
2. Salzmann, I.; Heimel, G.; Oehzelt, M.; Winkler, S.; Koch, N. Molecular Electrical Doping of Organic Semiconductors: Fundamental Mechanisms and Emerging Dopant Design Rules. *Acc. Chem. Res.* **2016**, *49*, 370–378.
3. Welch, G. C.; Coffin, R.; Peet, J.; Bazan, G. C. Band Gap Control in Conjugated Oligomers via Lewis Acids. *J. Am. Chem. Soc.* **2009**, *131*, 10802–10803.
4. Zalar, P.; Kuik, M.; Henson, Z. B.; Woellner, C.; Zhang, Y.; Sharenko, A.; Bazan, G. C.; Nguyen, T. Q. Increased Mobility Induced by Addition of a Lewis Acid to a Lewis Basic Conjugated Polymer. *Adv. Mater.* **2014**, *26*, 724–727.
5. Cheng, P.; Li, G.; Zhan, X.; Yang, Y. Next-Generation Organic Photovoltaics Based on Non-Fullerene Acceptors. *Nat. Photonics* **2018**, *12*, 131–142.
6. Hiramoto, M.; Fujiwara, H.; Yokoyama, M. Three-Layered Organic Solar Cell with a Photoactive Interlayer of Codeposited Pigments. *Appl. Phys. Lett.* **1991**, *58*, 1062–1064.
7. Yu, G.; Gao, J.; Hummelen, J. C.; Wudl, F.; Heeger, A. J. Polymer Photovoltaic Cells: Enhanced Efficiencies via a Network of Internal Donor-Acceptor Heterojunctions. *Science* **1995**, *270*, 1789–1791.
8. Yuan, J.; Zhang, H.; Zhang, R.; Wang, Y.; Hou, J.; Leclerc, M.; Zhan, X.; Huang, F.; Gao, F.; Zou, Y.; Li, Y. Reducing Voltage Losses in the A-DA′D-A Acceptor-Based Organic Solar Cells. *Chem* **2020**, *6*, 2147–2161.
9. Li, Y.; Xu, G.; Cui, C.; Li, Y. Flexible and Semitransparent Organic Solar Cells. *Adv. Energy Mater.* **2018**, *8*, 1701791.
10. Yan, C.; Barlow, S.; Wang, Z.; Yan, H.; Jen, A. K. Y.; Marder, S. R.; Zhan, X. Non-Fullerene Acceptors for Organic Solar Cells. *Nat. Rev. Mater.* **2018**, *3*, 18003.
11. Wadsworth, A.; Moser, M.; Marks, A.; Little, M. S.; Gasparini, N.; Brabec, C. J.; Baran, D.; McCulloch, I. Critical Review of the Molecular Design Progress in Non-Fullerene Electron Acceptors towards Commercially Viable Organic Solar Cells. *Chem. Soc. Rev.* **2019**, *48*, 1596–1625.
12. Lin, Y.; Zhan, X. Non-Fullerene Acceptors for Organic Photovoltaics: An Emerging Horizon. *Mater. Horiz.* **2014**, *1*, 470–488.
13. Lin, Y.; Wang, J.; Zhang, Z. G.; Bai, H.; Li, Y.; Zhu, D.; Zhan, X. An Electron Acceptor Challenging Fullerenes for Efficient Polymer Solar Cells. *Adv. Mater.* **2015**, *27*, 1170–1174.
14. Yang, Y.; Zhang, Z. G.; Bin, H.; Chen, S.; Gao, L.; Xue, L.; Yang, C.; Li, Y. Side-Chain Isomerization on an n-Type Organic Semiconductor ITIC Acceptor Makes 11.77% High Efficiency Polymer Solar Cells. *J. Am. Chem. Soc.* **2016**, *138*, 15011–15018.
15. Bauer, N.; Zhang, Q.; Rech, J. J.; Dai, S.; Peng, Z.; Ade, H.; Wang, J.; Zhan, X.; You, W. The Impact of Fluorination on Both Donor Polymer and Non-Fullerene Acceptor: The More Fluorine, the Merrier. *Nano Res.* **2019**, *12*, 2400–2405.
16. Cheng, P.; Yang, Y. Narrowing the Band Gap: The Key to High-Performance Organic Photovoltaics. *Acc. Chem. Res.* **2020**, *53*, 1218–1228.
17. Zhang, M.; Guo, X.; Ma, W.; Ade, H.; Hou, J. A Large-Bandgap Conjugated Polymer for Versatile Photovoltaic Applications with High Performance. *Adv. Mater.* **2015**, *27*, 4655–4660.
18. Fan, Q.; Zhu, Q.; Xu, Z.; Su, W.; Chen, J.; Wu, J.; Guo, X.; Ma, W.; Zhang, M.; Li, Y. Chlorine Substituted 2D-Conjugated Polymer for High-Performance Polymer Solar Cells with 13.1% Efficiency via Toluene Processing. *Nano Energy* **2018**, *48*, 413–420.
19. Guo, X.; Fan, Q.; Wu, J.; Li, G.; Peng, Z.; Su, W.; Lin, J.; Hou, L.; Qin, Y.; Ade, H.; Ye, L.; Zhang, M.; Li, Y. Optimized Active Layer Morphologies via Ternary Copolymerization of

DOI: 10.31635/ccschem.021.202100832
CCS Chem. **2021**, *3*, 1206–1216

Polymer Donors for 17.6% Efficiency Organic Solar Cells with Enhanced Fill Factor. *Angew. Chem. Int. Ed.* **2021**, *60*, 2322–2329.
20. Sun, C.; Pan, F.; Bin, H.; Zhang, J.; Xue, L.; Qiu, B.; Wei, Z.; Zhang, Z. G.; Li, Y. A Low Cost and High Performance Polymer Donor Material for Polymer Solar Cells. *Nat. Commun.* **2018**, *9*, 743.
21. Liu, Q.; Jiang, Y.; Jin, K.; Qin, J.; Xu, J.; Li, W.; Xiong, J.; Liu, J.; Xiao, Z.; Sun, K.; Yang, S.; Zhang, X.; Ding, L. 18% Efficiency Organic Solar Cells. *Chin. Sci. Bull.* **2020**, *65*, 272–275.
22. Ma, Y.; Cai, D.; Wan, S.; Wang, P.; Wang, J.; Zheng, Q. Ladder-Type Heteroheptacenes with Different Heterocycles for Nonfullerene Acceptors. *Angew. Chem. Int. Ed.* **2020**, *59*, 21627–21633.
23. Yuan, J.; Zhang, Y.; Zhou, L.; Zhang, G.; Yip, H.-L.; Lau, T.-K.; Lu, X.; Zhu, C.; Peng, H.; Johnson, P. A.; Leclerc, M.; Cao, Y.; Ulanski, J.; Li, Y.; Zou, Y. Single-Junction Organic Solar Cell with over 15% Efficiency Using Fused-Ring Acceptor with Electron-Deficient Core. *Joule* **2019**, *3*, 1140–1151.
24. Cui, Y.; Yao, H.; Zhang, J.; Zhang, T.; Wang, Y.; Hong, L.; Xian, K.; Xu, B.; Zhang, S.; Peng, J.; Wei, Z.; Gao, F.; Hou, J. Over 16% Efficiency Organic Photovoltaic Cells Enabled by a Chlorinated Acceptor with Increased Open-Circuit Voltages. *Nat. Commun.* **2019**, *10*, 2515.
25. Wang, J.; Zhan, X. Fused-Ring Electron Acceptors for Photovoltaics and Beyond. *Acc. Chem. Res.* **2021**, *54*, 132–143.
26. Zhang, Z.-G.; Qi, B.; Jin, Z.; Chi, D.; Qi, Z.; Li, Y.; Wang, J. Perylene Diimides: A Thickness-Insensitive Cathode Interlayer for High Performance Polymer Solar Cells. *Energy Environ. Sci.* **2014**, *7*, 1966–1973.
27. Yao, J.; Qiu, B.; Zhang, Z. G.; Xue, L.; Wang, R.; Zhang, C.; Chen, S.; Zhou, Q.; Sun, C.; Yang, C.; Xiao, M.; Meng, L.; Li, Y. Cathode Engineering with Perylene-Diimide Interlayer Enabling over 17% Efficiency Single-Junction Organic Solar Cells. *Nat. Commun.* **2020**, *11*, 2726.
28. Wu, Z.; Sun, C.; Dong, S.; Jiang, X. F.; Wu, S.; Wu, H.; Yip, H. L.; Huang, F.; Cao, Y. n-Type Water/Alcohol-Soluble Naphthalene Diimide-Based Conjugated Polymers for High-Performance Polymer Solar Cells. *J. Am. Chem. Soc.* **2016**, *138*, 2004–2013.
29. Boyle, C. J.; Upadhyaya, M.; Wang, P.; Renna, L. A.; Lu-Diaz, M.; Pyo Jeong, S.; Hight-Huf, N.; Korugic-Karasz, L.; Barnes, M. D.; Aksamija, Z.; Venkataraman, D. Tuning Charge Transport Dynamics via Clustering of Doping in Organic Semiconductor Thin Films. *Nat. Commun.* **2019**, *10*, 2827.
30. Peng, X.; Hu, L.; Qin, F.; Zhou, Y.; Chu, P. K. Low Work Function Surface Modifiers for Solution-Processed Electronics: A Review. *Adv. Mater. Interfaces* **2018**, *5*, 1701404.
31. Li, X.; Pan, F.; Sun, C.; Zhang, M.; Wang, Z.; Du, J.; Wang, J.; Xiao, M.; Xue, L.; Zhang, Z. G.; Zhang, C.; Liu, F.; Li, Y. Simplified Synthetic Routes for Low Cost and High Photovoltaic Performance *N*-Type Organic Semiconductor Acceptors. *Nat. Commun.* **2019**, *10*, 519.
32. Ge, J.; Xie, L.; Peng, R.; Fanady, B.; Huang, J.; Song, W.; Yan, T.; Zhang, W.; Ge, Z. 13.34 % Efficiency Non-Fullerene All-Small-Molecule Organic Solar Cells Enabled by Modulating the Crystallinity of Donors via a Fluorination Strategy. *Angew. Chem. Int. Ed.* **2020**, *59*, 2808–2815.
33. Bin, H.; Gao, L.; Zhang, Z. G.; Yang, Y.; Zhang, Y.; Zhang, C.; Chen, S.; Xue, L.; Yang, C.; Xiao, M.; Li, Y. 11.4% Efficiency Non-Fullerene Polymer Solar Cells with Trialkylsilyl Substituted 2D-Conjugated Polymer as Donor. *Nat. Commun.* **2016**, *7*, 13651.
34. Chang, Y.; Lau, T.-K.; Pan, M.-A.; Lu, X.; Yan, H.; Zhan, C. The Synergy of Host–Guest Nonfullerene Acceptors Enables 16%-Efficiency Polymer Solar Cells with Increased Open-Circuit Voltage and Fill-Factor. *Mater. Horiz.* **2019**, *6*, 2094–2102.
35. Pan, F.; Sun, C.; Li, Y.; Tang, D.; Zou, Y.; Li, X.; Bai, S.; Wei, X.; Lv, M.; Chen, X.; Li, Y. Solution-Processable n-Doped Graphene-Containing Cathode Interfacial Materials for High-Performance Organic Solar Cells. *Energy Environ. Sci.* **2019**, *12*, 3400–3411.
36. Xu, H.; Yuan, F.; Zhou, D.; Liao, X.; Chen, L.; Chen, Y. Hole Transport Layers for Organic Solar Cells: Recent Progress and Perspectives. *J. Mater. Chem. A* **2020**, *8*, 11478–11492.
37. Yurash, B.; Cao, D. X.; Brus, V. V.; Leifert, D.; Wang, M.; Dixon, A.; Seifrid, M.; Mansour, A. E.; Lungwitz, D.; Liu, T.; Santiago, P. J.; Graham, K. R.; Koch, N.; Bazan, G. C.; Nguyen, T. Q. Towards Understanding the Doping Mechanism of Organic Semiconductors by Lewis Acids. *Nat. Mater.* **2019**, *18*, 1327–1334.
38. Zalar, P.; Henson, Z. B.; Welch, G. C.; Bazan, G. C.; Nguyen, T. Q. Color Tuning in Polymer Light-Emitting Diodes with Lewis Acids. *Angew. Chem. Int. Ed.* **2012**, *51*, 7495–7498.
39. Yan, H.; Chen, J.; Zhou, K.; Tang, Y.; Meng, X.; Xu, X.; Ma, W. Lewis Acid Doping Induced Synergistic Effects on Electronic and Morphological Structure for Donor and Acceptor in Polymer Solar Cells. *Adv. Energy Mater.* **2018**, *8*, 1703672.
40. Welch, G. C.; Bazan, G. C. Lewis Acid Adducts of Narrow Band Gap Conjugated Polymers. *J. Am. Chem. Soc.* **2011**, *133*, 4632–4644.
41. Pingel, P.; Arvind, M.; Kölln, L.; Steyrleuthner, R.; Kraffert, F.; Behrends, J.; Janietz, S.; Neher, D. p-Type Doping of Poly (3-hexylthiophene) with the Strong Lewis Acid Tris(pentafluorophenyl)borane, *Adv. Electron. Mater.* **2016**, *2*, 1600204.
42. Paterson, A. F.; Tsetseris, L.; Li, R.; Basu, A.; Faber, H.; Emwas, A. H.; Panidi, J.; Fei, Z.; Niazi, M. R.; Anjum, D. H.; Heeney, M.; Anthopoulos, T. D. Addition of the Lewis Acid Zn $(C_6F_5)_2$ Enables Organic Transistors with a Maximum Hole Mobility in Excess of 20 cm^2/Vs. *Adv. Mater.* **2019**, *31*, 1900871.
43. Panidi, J.; Paterson, A. F.; Khim, D.; Fei, Z.; Han, Y.; Tsetseris, L.; Vourlias, G.; Patsalas, P. A.; Heeney, M.; Anthopoulos, T. D. Remarkable Enhancement of the Hole Mobility in Several Organic Small-Molecules, Polymers, and Small-Molecule: Polymer Blend Transistors by Simple Admixing of the Lewis Acid p-Dopant $B(C_6F_5)_3$. *Adv. Sci.* **2018**, *5*, 1700290.
44. Han, Y.; Barnes, G.; Lin, Y.-H.; Martin, J.; Al-Hashimi, M.; AlQaradawi, S. Y.; Anthopoulos, T. D.; Heeney, M. Doping of Large Ionization Potential Indenopyrazine Polymers via Lewis Acid Complexation with Tris(pentafluorophenyl)borane: A Simple Method for Improving the Performance of

DOI: 10.31635/ccschem.021.202100832
CCS Chem. **2021**, *3*, 1206–1216

Organic Thin-Film Transistors. *Chem. Mater.* **2016**, *28*, 8016–8024.
45. Palermo, V.; Palma, M.; Samorì, P. Electronic Characterization of Organic Thin Films by Kelvin Probe Force Microscopy. *Adv. Mater.* **2006**, *18*, 145–164.
46. Kahn, A. Fermi Level, Work Function and Vacuum Level. *Mater. Horiz.* **2016**, *3*, 7–10.
47. Melitz, W.; Shen, J.; Kummel, A. C.; Lee, S. Kelvin Probe Force Microscopy and Its Application. *Surf. Sci. Rep.* **2011**, *66*, 1–27.
48. Shikler, R.; Meoded, T.; Fried, N.; Mishori, B.; Rosenwaks, Y. Two-Dimensional Surface Band Structure of Operating Light Emitting Devices. *J. Appl. Phys.* **1999**, *86*, 107–113.
49. Li, T.; Lipatov, A.; Lu, H.; Lee, H.; Lee, J. W.; Torun, E.; Wirtz, L.; Eom, C. B.; Iniguez, J.; Sinitskii, A.; Gruverman, A. Optical Control of Polarization in Ferroelectric Heterostructures. *Nat. Commun.* **2018**, *9*, 3344.
50. Lin, Y.; He, Q.; Zhao, F.; Huo, L.; Mai, J.; Lu, X.; Su, C. J.; Li, T.; Wang, J.; Zhu, J.; Sun, Y.; Wang, C.; Zhan, X. A Facile Planar Fused-Ring Electron Acceptor for As-Cast Polymer Solar Cells with 8.71% Efficiency. *J. Am. Chem. Soc.* **2016**, *138*, 2973–2976.
51. Liu, S.; Yuan, J.; Deng, W.; Luo, M.; Xie, Y.; Liang, Q.; Zou, Y.; He, Z.; Wu, H.; Cao, Y. High-Efficiency Organic Solar Cells with Low Non-Radiative Recombination Loss and Low Energetic Disorder. *Nat. Photonics* **2020**, *14*, 300–305.
52. Jiang, K.; Wei, Q.; Lai, J. Y. L.; Peng, Z.; Kim, H. K.; Yuan, J.; Ye, L.; Ade, H.; Zou, Y.; Yan, H. Alkyl Chain Tuning of Small Molecule Acceptors for Efficient Organic Solar Cells. *Joule* **2019**, *3*, 3020–3033.
53. Cui, Y.; Yao, H.; Zhang, J.; Xian, K.; Zhang, T.; Hong, L.; Wang, Y.; Xu, Y.; Ma, K.; An, C.; He, C.; Wei, Z.; Gao, F.; Hou, J. Single-Junction Organic Photovoltaic Cells with Approaching 18% Efficiency. *Adv. Mater.* **2020**, *32*, 1908205.
54. Sun, H.; Liu, T.; Yu, J.; Lau, T.-K.; Zhang, G.; Zhang, Y.; Su, M.; Tang, Y.; Ma, R.; Liu, B.; Liang, J.; Feng, K.; Lu, X.; Guo, X.; Gao, F.; Yan, H. A Monothiophene Unit Incorporating Both Fluoro and Ester Substitution Enabling High-Performance Donor Polymers for Non-Fullerene Solar Cells with 16.4% Efficiency. *Energy Environ. Sci.* **2019**, *12*, 3328–3337.
55. Zhang, D.; Li, Q.; Zhang, J.; Wang, J.; Zhang, X.; Wang, R.; Zhou, J.; Wei, Z.; Zhang, C.; Zhou, H.; Zhang, Y. Control of Nanomorphology in Fullerene-Free Organic Solar Cells by Lewis Acid Doping with Enhanced Photovoltaic Efficiency. *ACS Appl. Mater. Interfaces* **2020**, *12*, 667–677.
56. Chen, Z.; Tang, Y.; Lin, B.; Zhao, H.; Li, T.; Min, T.; Yan, H.; Ma, W. Probe and Control of the Tiny Amounts of Dopants in BHJ Film Enable Higher Performance of Polymer Solar Cells. *ACS Appl. Mater. Interfaces* **2020**, *12*, 25115–25124.
57. Hao Huang, H.; Guo, Q.; Feng, S.; Zhang, C.; Bi, Z.; Xue, W.; Yang, J.; Song, J.; Li, C.; Xu, X.; Tang, Z.; Ma, W.; Bo, Z. Noncovalently Fused-Ring Electron Acceptors with Near-Infrared Absorption for High-Performance Organic Solar Cells. *Nat. Commun.* **2019**, *10*, 3038.
58. Gao, H.-H.; Sun, Y.; Cai, Y.; Wan, X.; Meng, L.; Ke, X.; Li, S.; Zhang, Y.; Xia, R.; Zheng, N.; Xie, Z.; Li, C.; Zhang, M.; Yip, H.-L.; Cao, Y.; Chen, Y. Achieving Both Enhanced Voltage and Current through Fine-Tuning Molecular Backbone and Morphology Control in Organic Solar Cells. *Adv. Energy Mater.* **2019**, *9*, 1901024.
59. Glaz, M. S.; Biberdorf, J. D.; Nguyen, M. T.; Travis, J. J.; Holliday, B. J.; Vanden Bout, D. A. Perylene Diimide Functionalized Polynorbornene: A Macromolecular Scaffold for Supramolecular Self-Assembly. *J. Mater. Chem. C* **2013**, *1*, 8060–8065.
60. Jiang, Y.; Huang, W.; Schmalle, H. W.; Blacque, O.; Fox, T.; Berke, H. Structural Evidence for Lewis Acid Triggered Nitrosyl Bending in Rhenium(-I) Chloro Catalysts for Alkene Hydrogenation Reactions. *Eur. J. Inorg. Chem.* **2014**, *2014*, 140–147.
61. Wanglee, Y. J.; Hu, J.; White, R. E.; Lee, M. Y.; Stewart, S. M.; Perrotin, P.; Scott, S. L. Borane-Induced Dehydration of Silica and the Ensuing Water-Catalyzed Grafting of $B(C_6F_5)_3$ to Give a Supported, Single-Site Lewis Acid, $\equiv SiOB(C_6F_5)_2$. *J. Am. Chem. Soc.* **2012**, *134*, 355–366.

DOI: 10.31635/ccschem.021.202100832
CCS Chem. **2021**, *3*, 1206–1216